Metamaterial-Substrate Antenna Array for MIMO Communication System

Prathaban Mookiah, *Student Member, IEEE*, and Kapil R. Dandekar, *Senior Member, IEEE*

***Abstract*—We demonstrate how a magnetic permeability enhanced metamaterial can enhance the antenna array of a multiple-input multiple-output (MIMO) communication system. The performance of a rectangular patch antenna array on a metamaterial substrate was studied relative to a similar array constructed on a conventional FR4 substrate. Differently spaced arrays were analytically compared using array correlation coefficients and mean effective gain as performance metrics. Achievable channel capacity were obtained through channel measurements made on a MIMO testbed. While results show that arrays on conventional FR4 substrates have higher capacity due to gain and efficiency factors, arrays can be made smaller, and have less mutual coupling and correlation coefficients, when using a metamaterial substrate, but the antenna built on the metamaterial substrate can be made more efficient through the use of better host materials. This was reflected in the analysis of both antenna arrays normalized to remove efficiency and gain differences where they showed similar performances. Hence, metamaterial substrates are a cost-effective solution when antenna miniaturization is a key design criteria compared to conventional substrates that achieve the same miniaturization factor without significantly sacrificing performance.**

***Index Terms*—Channel measurements, multiple-input multiple-output (MIMO) systems, mean effective gain, metamaterial substrate.**

I. Introduction

Wireless communication systems have become pervasive and ubiquitous to the point where data rate and quality of service requirements have become comparable to those of wired communication systems. Next-generation wireless systems incorporate multiple-input multiple-output (MIMO) techniques to achieve their performance goals. MIMO systems promise higher channel capacities compared to single antenna systems by exploiting the spatial characteristics of the multipath wireless propagation channel [1]. The theoretical performance gain achievable by MIMO systems is limited due to a number of practical design factors, including the design of the antenna array and the amount of inter-array element mutual coupling. While mutual coupling can improve performance in certain environments by creating pattern diversity [2], increased correlation between the received signals in other environments can degrade performance [3], [4]. Though increasing the spacing between array elements can alleviate mutual coupling, accommodating multiple antennas with large inter-element spacing in modern consumer devices may be impossible due to stringent space constraints. In order to meet such demanding, and often contradictory design criteria, antenna designers have been constantly driven to seek better antenna designs and materials on which to build antenna systems.

A plethora of antenna miniaturization techniques have been reported in literature. Fractal antenna techniques have been extensively applied to miniaturize different kinds of wire antenna with reasonable outcomes [5]. Microstrip patch antenna size reduction has been achieved through the use of high dielectric materials [6]. Changing the current path by introducing slots on the resonating surface has been reported in [7]. Other constructions for reduced size patch antennas include multi-layer patch antennas [8], planar inverted F antennas [9] and quarter-wave patches [10]. Electromagnetic band-gap materials have been shown to significantly reduce substrate thicknesses and are being actively applied for different antenna structures [11]. A completely different approach to antenna miniaturization is the application of genetic algorithms in antenna design.

Metamaterials are a broad class of synthetic materials that could be engineered to wield permittivity and permeability characteristics to system requirements [13], [14]. By embedding specific structures (usually periodic structures) in some host media (usually a dielectric substrate), the resulting material can be tailored to exhibit desirable characteristics. These materials have drawn a lot of interest in the antenna community due to their promising features. Metamaterials have been extensively applied for antenna applications recently to achieve antenna miniaturization [15], improved directivity [16], beam scanning [17], and beamwidth control [17].

A novel application of metamaterials has been found in enhancing the magnetic permeability of otherwise nonmagnetic materials [18], [19]. It is well known that antennas suffer from poor efficiency when their sizes go below $\lambda/10$ where λ is the operating wavelength, a fact that has been a major impediment in using high dielectric materials to miniaturize antennas, but magnetic permeability enhanced metamaterials can provide a more balanced solution to this problem since these materials can miniaturize antennas by not only scaling down the wavelength with their permittivity, but also with their high permeability, resulting in a significant size reduction while operating at acceptable efficiencies.

Manuscript received October 24, 2008; revised March 04, 2009. First published July 10, 2009; current version published October 07, 2009. Preliminary simulation results related to this work were submitted and accepted for presentation at the *IEEE Global Communications Conference*, New Orleans, LA, Nov. 2008.

The authors are with the Department of Electrical and Computer Engineering, Drexel University, Philadelphia, PA 19104 USA (e-mail: mprathap@drexel.edu; dandekar@ece.drexel.edu).

Color versions of one or more of the figures in this paper are available online at http://ieeexplore.ieee.org.

Digital Object Identifier 10.1109/TAP.2009.2028638

In this paper, we quantify the performance of a miniaturized rectangular patch antenna array built on a magnetic permeability enhanced metamaterial substrate for a 2×2 MIMO communications system using spatial multiplexing. Channel matrices were measured in different indoor propagation environments for different inter-element spacings at a carrier frequency of 2.48 GHz. The measurements were repeated with a similar antenna array built on a conventional FR4 substrate. Comparisons are made between the two systems in terms of mean effective gain (MEG), envelope correlation coefficients, measured channel capacities, and array physical footprint on a mobile device.

Following this introduction, we discuss the design of the magnetic permeability enhanced metamaterial substrate in Section II. Section III presents the design, construction and measured characteristics of the antenna array built on the metamaterial substrate. Equipped with these antenna measurements, we proceed to analyze, through simulations, the performance of the antenna array in different radio propagation scenarios, first by studying the correlation coefficients in Section IV and mean effective gain in Section V. The results of actual measurements are presented and discussed in Section VI before we draw our conclusions in Section VII.

II. Metamaterial Substrate Design

Inside a dielectric material, the free space wavelength of an antenna is scaled down by a factor of $\sqrt{\mu_r \epsilon_r}$, where ϵ_r is the relative electric permittivity and μ_r is the relative magnetic permeability of the material. Thus, the size of an antenna can be significantly reduced by choosing a high ϵ_r or high μ_r material. Though miniaturization can be achieved using high ϵ_r materials, it comes at the cost of increased dielectric losses that can significantly affect antenna efficiency [6]. On the other hand, materials that exhibit a high μ_r in the microwave region do not exist in nature and designers have been compelled to use lossy high ϵ_r materials when antenna miniaturization is a key design requirement. Fortunately materials that exhibit high μ_r, or magnetic permeability enhanced metamaterials, can now be artificially engineered to lead to smaller antennas without compromising other design criteria [19].

Magnetic permeability enhanced metamaterials are constructed by stacking up unit cells that can store magnetic energy by virtue of their structure. A unit cell for the material used in this paper contains an inductive spiral loop embedded in a host dielectric material as shown in Fig. 1. Magnetic energy storage is created in the unit cell when a magnetic field passes normal to the plane of the spiral, inducing a current in the loop. This phenomenon effectively creates an inductance within the host substrate material. The material is formed by stacking up these unit cells uniformly in three dimension. A resonance behavior is generated at frequencies dictated by the inductance of the loop and capacitances that exist between adjacent arms in the loop. Thus at resonance, a significant net magnetic energy storage is induced within the 3-D structure and thus the magnetic permeability of the otherwise nonmagnetic substrate material is enhanced. In order to realize a miniaturized antenna, it is therefore necessary to match the resonance frequency of the antenna and the material. The resonance frequency of this structure can be controlled by tuning the spiral and substrate dimensions.

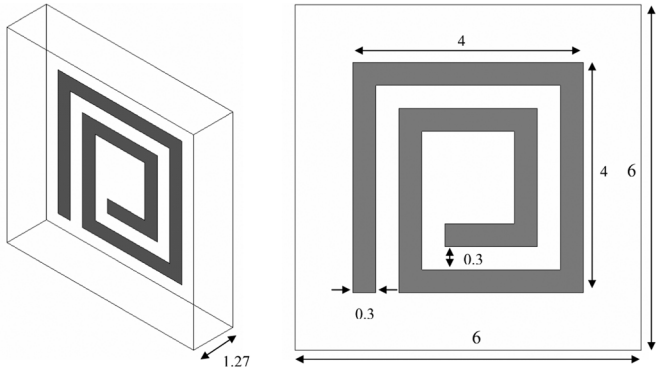

Fig. 1. Structure of metamaterial unit cell containing spiral loop embedded in a dielectric substrate (all units are in mm). The dielectric substrate is FR4 ($\epsilon_r = 4.4, \mu_r = 1$, loss tangent $\tan\delta = 0.02$).

The resonance frequency for the intended antenna design is 2.48 GHz. Therefore the unit cell structure is designed to resonate at this frequency, consistent with the antenna resonance frequency. The unit cell structure designed to resonate in the 2.48 GHz band is shown in Fig. 1 along with its dimensions. FR4 ($\epsilon_r = 4.4, \mu_r = 1$, loss tangent $\tan\delta = 0.02$) was chosen as the host material for the metamaterial substrate. Initial simulations of the unit cell and the stacked 3-D structure were carried out using the finite-element method software HFSS [20]. Bulk material properties of this substrate were extracted from the simulated S parameters as described in [21]. The extracted ϵ_r and μ_r values around the 2.48 GHz band is shown in Fig. 2(a). The effective μ_r was found to be approximately 4.2 in the direction perpendicular to the plane of the unit cell. This substrate also experiences an enhancement in permittivity due its geometry [19]. The extracted effective ϵ_r was 9.7. The resulting electric and magnetic $\tan\delta$ values are plotted in Fig. 2(b). The resulting electric and magnetic $\tan\delta$ are 0.2 and 0.05, respectively, at the design frequency. These values imply a lossy substrate leading to poor antenna efficiencies. We discuss this problem and possible ways to improve antenna performance in Section III-C.

The unit cells were fabricated using a T-Tech QC5000 milling machine. Unit cells belonging to the same plane in the 3-D structure were milled together on a single FR4 block and these blocks were held together using tiny plastic screws at either ends of the blocks. The misalignment caused by the unit cells was limited to 0.1 mm which corresponds to the tolerance of the milling machine. The antenna and ground plane were cut out from a 0.07-mm-thick copper sheet using our milling machine and was affixed to the substrate using a thin coating of polymer based industrial adhesive.

III. Antenna Design

The antenna geometry used in this study is a rectangular patch antenna with a recessed microstrip feed line [22], backed by a ground plane and operating in the TM_{010} mode built on the metamaterial substrate. Current is induced in the spiral loop only by magnetic fields oriented in a direction perpendicular to the plane of the spiral. Hence, magnetic permeability enhancement is unidirectional in the substrate. Since the magnetic field in the

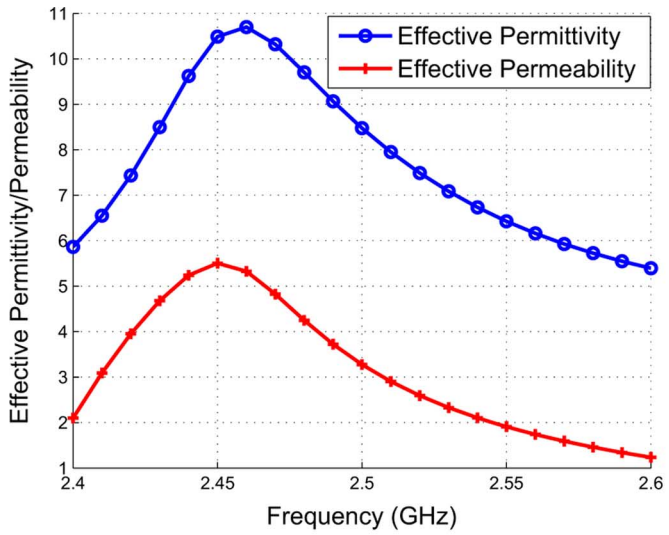

(a)

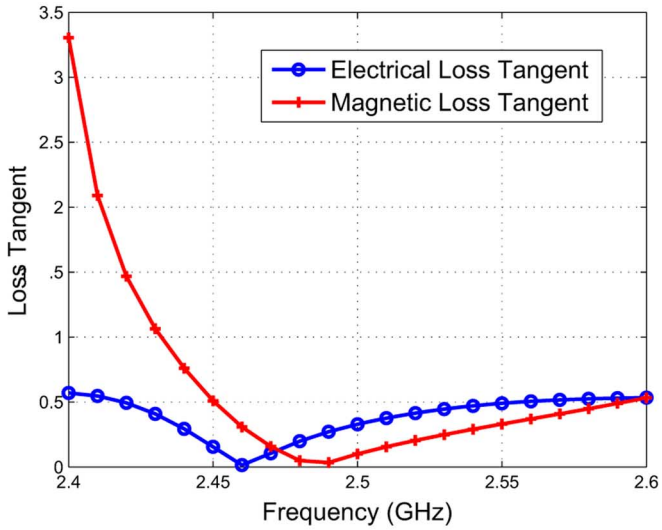

(b)

Fig. 2. Effective material parameters around the resonance frequency of 2.48 GHz from HFSS simulations. (a) Effective permittivity (ϵ_r) and permeability (μ_r). (b) Electrical and magnetic loss tangents $(\tan\delta)$.

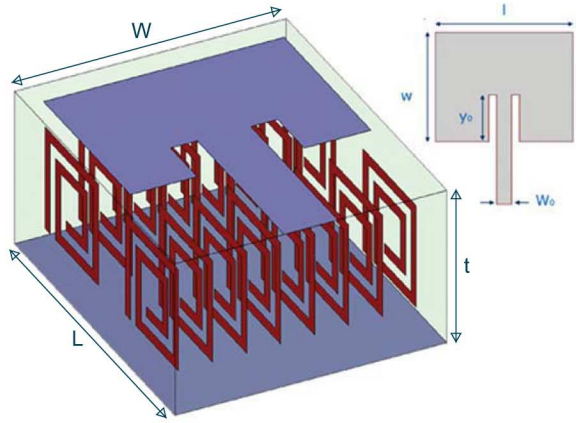

(a)

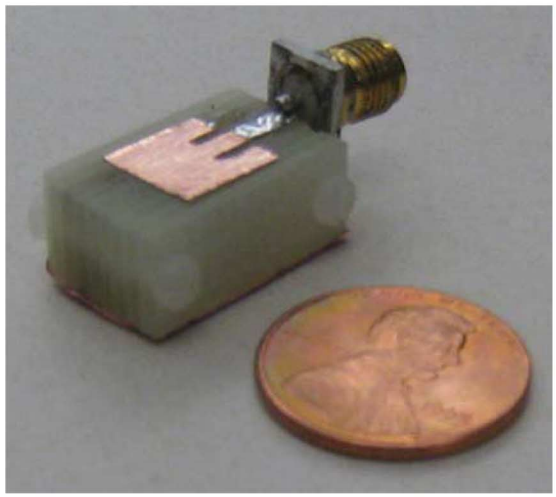

(b)

Fig. 3. (a) Schematic of the rectangular patch antenna built on the magnetic permeability enhanced metamaterial substrate. The dimensions are listed in Table I. (b) Fabricated metamaterial-substrate antenna structure.

near field of a rectangular patch antenna would be in a direction perpendicular to its radiating edge, this antenna design can fully utilize the available permeability in this direction.

The structural details of an antenna element on the 3-D metamaterial substrate and a built prototype are shown in Fig. 3. A picture of the antenna array mounted on the testbed used for channel measurements is shown in Fig. 4. The relevant substrate and antenna dimensions are shown in Table I. Dimensions are also shown in Table I for similar antenna built on a regular FR4 substrate that was used as a reference to compare the performance of our metamaterial-substrate antenna. The designed metamaterial-substrate antenna achieved a miniaturization factor of approximately 3 in the radiation edge length compared to a rectangular patch antenna operating at the same frequency built on a conventional FR4 substrate. Also, a significant 90% reduction in the area occupied by the antenna plane was achieved. However, due to the higher thickness of the metamaterial substrate, the entire volume for a single antenna on a metamaterial substrate was approximately 37% less than that of a conventional FR4 substrate.

A. *Bandwidth and Gain*

Fig. 5 shows the measured return loss characteristics of the designed antenna. The -10-dB bandwidth of this antenna is approximately 50 MHz. This bandwidth is comparable to that of an antenna built on a conventional FR4 substrate.

Fig. 6 shows the measured gain of the metamaterial and FR4 antennas in the elevation and azimuth planes. The conventional FR4 substrate antenna has 6 dB more gain than the metamaterial-substrate antenna in the elevation plane and approximately 2 dB more gain in the azimuth plane. Although the difference in gain is significant in the elevation plane, the primary contribution to the difference in communication system performance between the two antennas would be due to gain differences in the azimuth plane [23]. These gain differences between the antennas can be attributed to two factors.

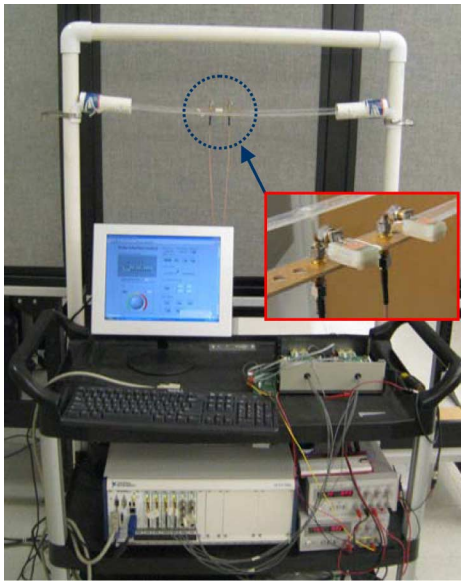

Fig. 4. View of the metamaterial-substrate antenna array mounted on the HYDRA testbed during channel measurements.

TABLE I
SUBSTRATE AND ANTENNA DIMENSIONS

Dimension (mm)	Metamaterial	FR4
L	18	45
W	10	40
l	9	33
w	9	29
y_0	3	6
W_0	2	5
t	8	1.27

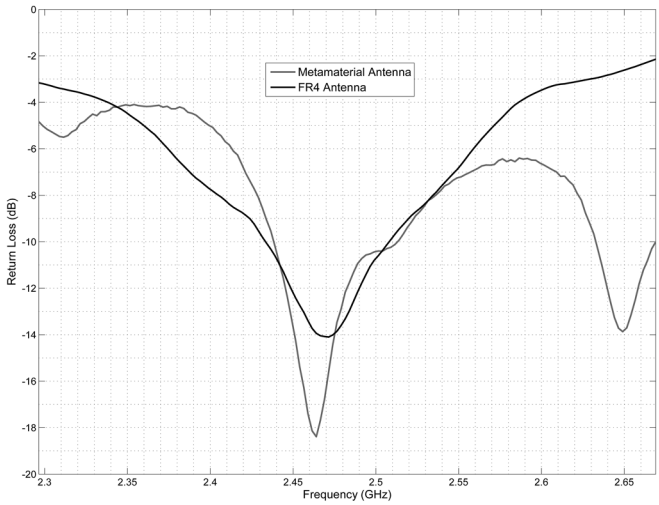

Fig. 5. Measured return loss characteristics for the metamaterial and FR4 substrate antennas.

The primary reason for the gain differences is the smaller efficiency of the metamaterial-substrate antenna as discussed in the next section. Second, the metamaterial-substrate antenna has a much smaller ground plane compared to the conventional FR4 substrate antenna which leads to more fringing effects and a reduction in directivity in the elevation plane as seen in 6(a). To

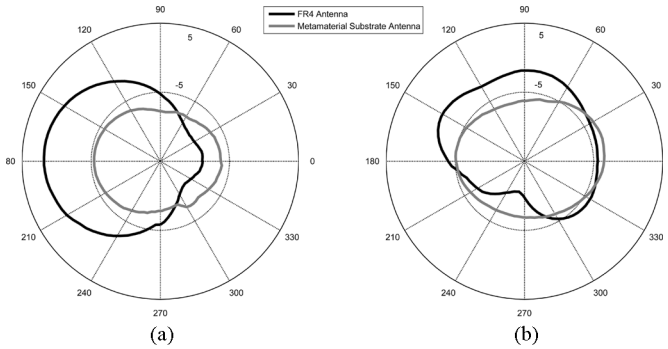

Fig. 6. Measured gain in the (a) elevation plane ($\phi = 0^o$) and (b) azimuth plane ($\theta = 90^o$) for metamaterial and FR4 substrate antennas. The spacing between the antenna elements is 60 mm($\lambda/2$).

study the effect of substrate size, the metamaterial-substrate antenna was constructed on a larger metamaterial substrate with the substrate length and width equal to that of the FR4 antenna substrate. Therefore the ground plane for this antenna was equal in size to that of the FR4 antenna. The antenna is shown in Fig. 7(a). The measured radiation pattern in the elevation plane for this antenna shown in Fig. 7(b) shows that the peak gain in the this plane for this metamaterial-substrate antenna was around -2 dBi. This corresponds to a 3-dB gain improvement compared to that of the original metamaterial-substrate antenna design with a smaller substrate. The large back-lobe that was present in the original metamaterial-substrate antenna as seen in Fig. 6(a) was significantly suppressed for this design. The measured azimuthal gain did not show any significant differences in gain values between the two antennas with different substrate sizes.

It is important that the azimuth gain does not deteriorate within the usage bandwidth as the azimuth plane gain has a more significant effect on capacity performance since multipath signal propagation in indoor environments (such as the ones used for channel measurements in this paper) happens mostly in this plane [23]. Table II lists the peak gain in the elevation and azimuth planes for frequencies around 2.484 GHz at which the channel measurements were performed. As seen in the table, the designed antenna's gain characteristics does not deteriorate in this frequency region. The performance dependence on the azimuthal gain pattern also justifies the sacrifice made in the elevation plane gain due to a smaller ground plane in order to achieve a smaller antenna footprint.

B. Cross-Polarization Discrimination

Cross-polarization discrimination (XPD) quantifies the degree of the sense of polarization of a linearly polarized antenna. The XPD of an antenna is given by

$$\mathrm{XPD} = \frac{\int_0^{2\pi}\int_{-\pi/2}^{\pi/2} G_\theta(\theta,\phi)\cos\theta d\theta d\phi}{\int_0^{2\pi}\int_{-\pi/2}^{\pi/2} G_\phi(\theta,\phi)\cos\theta d\theta d\phi} \quad (1)$$

where $G_\theta(\theta,\phi)$ and $G_\phi(\theta,\phi)$ are the θ and ϕ components of the antenna gain pattern. The computed XPD values for the metamaterial substrate and FR4 antennas are given in Table III when the antennas are placed at different spacings in an array.

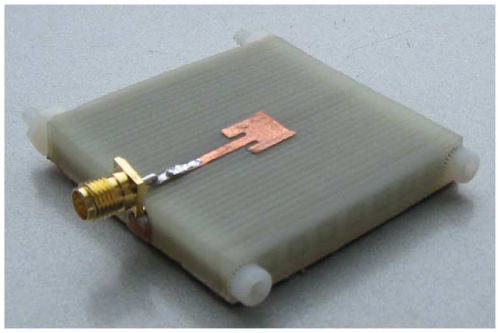

(a)

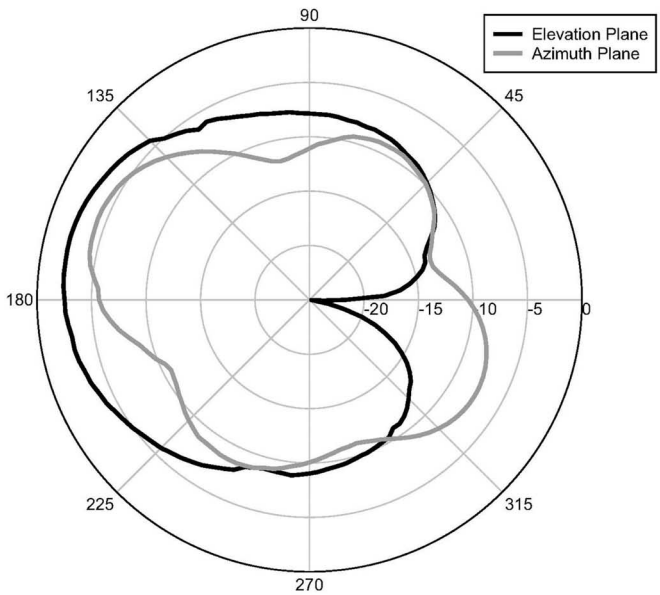

(b)

Fig. 7. (a) Antenna constructed on a larger metamaterial substrate in order to study the effect of having a large ground plane. (b) Elevation and azimuth radiation patterns of the metamaterial-substrate antenna with the larger ground plane.

TABLE II
PEAK GAINS AT DIFFERENT FREQUENCIES AROUND 2.2484 GHz IN THE ELEVATION AND AZIMUTHAL PLANES

Frequency (GHz)	Peak Elevation Gain [dBi]	Peak Azimuth Gain [dBi]
2.464	-4.5	-3.0
2.476	-5.6	-3.5
2.496	-4.5	-2.5
2.504	-4.2	-2.2

TABLE III
XPD FOR DIFFERENT ANTENNA ARRAY CONFIGURATIONS

Antenna Configuration	XPD [dB]
Metamaterial-Substrate Antenna at 0.05λ	7.8
Metamaterial-Substrate Antenna at 0.5λ	4.2
FR4 Antenna at 0.05λ	7.3
FR4 Antenna at 0.5λ	2.7

The antennas are linearly polarized as expected of a rectangular microstrip patch antenna and XPD decreases with inter-element spacing for both antenna types. As seen from the table, less polarization distortion occurs due to the presence of the other antenna elements in the array for the metamaterial-substrate antenna compared to the FR4 antenna. This can be explained by the unidirectional substrate enhancement that "suppresses" the cross-polar fields generated in the substrate, resulting in less cross-polararization coupling.

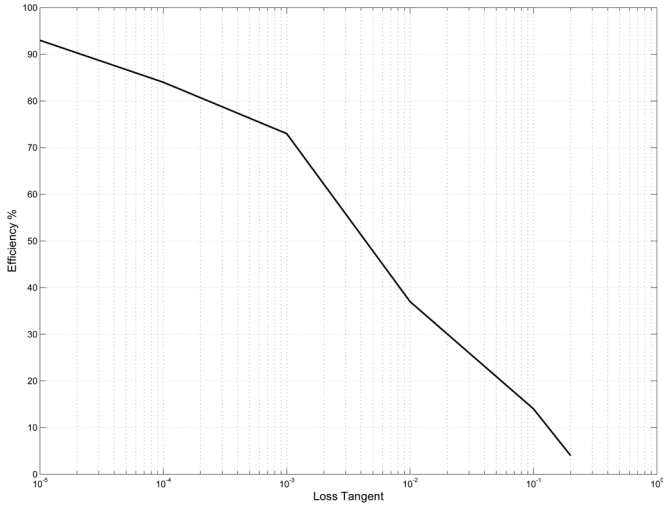

Fig. 8. Predicted radiation efficiency of the metamaterial-substrate antenna for different host substrate $\tan\delta$ with the other material properties remaining the same as that of FR4.

C. *Efficiency*

The measured efficiency for the metamaterial-substrate antenna and FR4 antenna were 30% and 48%, respectively. In addition to the losses due to surface waves excited in the substrate, which contributes to losses in both antennas, the current induced in the inductive loop in each unit cell contributes to ohmic losses in the metamaterial substrate. Additionally the capacitive losses in the metamaterial host medium is also increased due to the increased thickness of the stacked substrate structure. The electric and magnetic $\tan\delta$ determined in Section II demonstrate these results. While, at first look, this difference in efficiency may discourage the use of a metamaterial substrate, this difference should be viewed in light of several other factors. Fig. 8 shows the simulated efficiencies obtainable with the metamaterial-substrate antenna for different $\tan\delta$ with the other host material properties being the same as that of FR4. It can be seen that the problem of lower efficiency is mainly due to the lossy nature of the FR4 substrate. Therefore, the problem of efficiency can be addressed by choosing a low loss host material.

Also a simple calculation based on the miniaturization factor described in a preceding paragraph reveals that it requires a conventional substrate with an ϵ_r value of 45 to achieve the miniaturization factor achieved by the metamaterial substrate. There a two reasons for why a metamaterial substrate would be a better choice than a material with such a high ϵ_r. The theoretical maximum efficiency achievable by a microstrip patch antenna decreases significantly with ϵ_r due to the high dielectric losses incurred in such a material. The maximum efficiency predicted by [6] for an antenna built on a material with an ϵ_r of 45 and $\tan\delta$ of 0.0001 would be around 35% which is similar to that of the efficiency achieved by the metamaterial substrate built

on FR4 as the host substrate. As predicted by Fig. 8, a more efficient antenna can be realized by building the substrate on a lower ϵ_r but less lossy host material. The second reason is that low-loss, high-ϵ_r materials can be prohibitively expensive since they are usually composites made of different materials. Cheaper polymer based alternatives have much higher dielectric losses compared to the metamaterial substrate $(\tan\delta > 0.02)$ leading to efficiencies on the order of 5%–15% [6]. Hence, when miniaturization is a key design requirement, the metamaterial substrate is an efficient and cost-effective solution.

IV. Analysis of Correlation Characteristics

The signal correlation at the receiver is an important factor that affects the operation of a MIMO system. Mutual coupling between the antenna elements as well as the radio propagation environment contribute to signal correlation. In this section we quantify signal correlation using two metrics: mutual coupling between the antenna elements and the correlation coefficient.

Higher mutual coupling between the antenna elements in a MIMO system leads to higher correlation between the received signals and thus lower system performance. For arrays on both substrates considered in this paper, the mutual coupling between array elements was analyzed in terms of the isolation (S_{21}) between them. Isolation between the antenna elements was measured using a vector network analyzer in free space with the antennas mounted on the testbed as shown in Fig. 4. The measured isolations for the metamaterial-substrate antenna array and the conventional FR4 antenna array are shown in Fig. 10. The result shows a difference of 15 dB in isolation between the metamaterial and FR4 antenna arrays at very low inter element spacing. This difference drops to around 10 dB for higher spacing. This trend implies that the received signals will be significantly less correlated for the metamaterial-substrate antenna compared to the FR4 antenna for a given spacing. Another interesting observation is that the isolation does not vary as much with inter-element spacing for the metamaterial-substrate antenna; the difference in isolation between $\lambda/20$ and $7\lambda/10$ is 10 dB whereas the isolation varies by 16 dB for the FR4 antennas.

The correlation coefficient between the receiving antenna elements in a given environment takes into account both the antenna's radiation pattern as well as the power angular spectrum (PAS) of the environment and is thus an effective parameter to characterize the degree of signal degradation due to antenna and environmental correlation effects. The correlation coefficient between the antenna elements in a MIMO array is given by equation (2), shown at the bottom of the page [24], where XPR is the cross polarization power ratio, $P_\theta(\theta,\phi)$ and $P_\phi(\theta,\phi)$ are the θ and ϕ components of the PAS of the incident waves and $E_{\theta k}(\theta,\phi)$, $E_{\phi k}(\theta,\phi)$ are the θ and ϕ components of the kth antenna's complex electric field envelopes, x is the distance between the two antenna elements, and β is the wave number.

TABLE IV
Correlation Coefficients

Antenna Type	$\lambda/20$ spacing	$\lambda/2$ spacing
Metamaterial Substrate	0.22	0.01
FR4	0.79	0.04

The propagation environment is specified by the PAS of the vertically and horizontally polarized incident radio waves. The power angular spectrum of the vertically and horizontally polarized received signals are assumed to be distributed uniformly in azimuth and distributed as a Gaussian function in elevation which is consistent with the measured results reported in [25] for an indoor environment. Therefore, the distributions corresponding to PAS are given by

$$P_\theta(\theta,\phi) = A_\theta \exp\left[-\frac{(\theta-\theta_v)^2}{2\sigma_v^2}\right], \quad \theta \in \left[-\frac{\pi}{2},\frac{\pi}{2}\right] \tag{3}$$

$$P_\phi(\theta,\phi) = A_\phi \exp\left[-\frac{(\theta-\theta_h)^2}{2\sigma_h^2}\right], \quad \theta \in \left[-\frac{\pi}{2},\frac{\pi}{2}\right] \tag{4}$$

where A_θ and A_ϕ are constants that satisfy the condition that the area under both the curves sum to 1, θ_v and θ_h are the means and σ_v and σ_h are the standard deviations of the θ and ϕ polarized components, respectively. The correlation coefficients for the two antenna array under different element spacings in an environment characterized by the following parameters are listed in Table IV: $m_V = m_V = 3^o$, $\sigma_V = \sigma_H = 10^o$, and $\mathrm{XPR} = 7$ dB. The choice of these values was based on the measurement results reported for an indoor picocell in [25]. The closely spaced FR4 antennas experience higher correlation than the metamaterial-substrate antennas. The FR4 antenna is heavily correlated at closer spacings and correlation improvement is significant with increased spacing, whereas the metamaterial-substrate antenna is reasonably uncorrelated even at closer inter-element spacings. Thus, as a result of the high inter-element isolation between the elements, the metamaterial antenna array remains significantly less correlated at closer inter-element spacings in a typical indoor propagation environment such as the one described here.

V. Mean Effective Gain Analysis

Though antenna gain is a good measure for an antenna's performance in a stationary wireless communication system, it does not give complete information to the system designer on how well the antenna will perform in a mobile system due to the randomness of the multipaths. The mean effective gain (MEG) of an antenna has been used as a possible measure to evaluate an antenna's performance in such mobile wireless channels [26].

$$\rho_e = \frac{\left[\left|\int\{\mathrm{XPR}.E_{\theta 1}(\theta,\phi)E^*_{\theta 2}(\theta,\phi)P_\theta(\theta,\phi) + E_{\phi 1}(\theta,\phi)E^*_{\phi 2}(\theta,\phi)P_\phi(\theta,\phi)\}\exp^{-j\beta x}\, d\phi d\theta\right|^2\right]}{\left[\begin{array}{c}\int\{\mathrm{XPR}\cdot E_{\theta 1}(\theta,\phi)E^*_{\theta 1}(\theta,\phi)P_\theta(\theta,\phi) + E_{\phi 1}(\theta,\phi)E^*_{\phi 1}(\theta,\phi)P_\phi(\theta,\phi)\}d\phi d\theta \\ \times\int\{XPR.E_{\theta 2}(\theta,\phi)E^*_{\theta 2}(\theta,\phi)P_\theta(\theta,\phi) + E_{\phi 2}(\theta,\phi)E^*_{\phi 2}(\theta,\phi)P_\phi(\theta,\phi)\}d\phi d\theta\end{array}\right]} \tag{2}$$

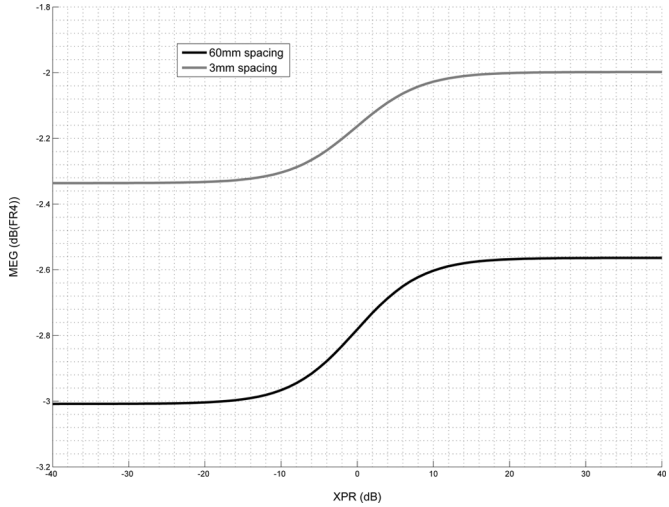

Fig. 9. MEG variation for the metamaterial-substrate antenna with XPR. The MEG values are referenced to the FR4 substrate antenna.

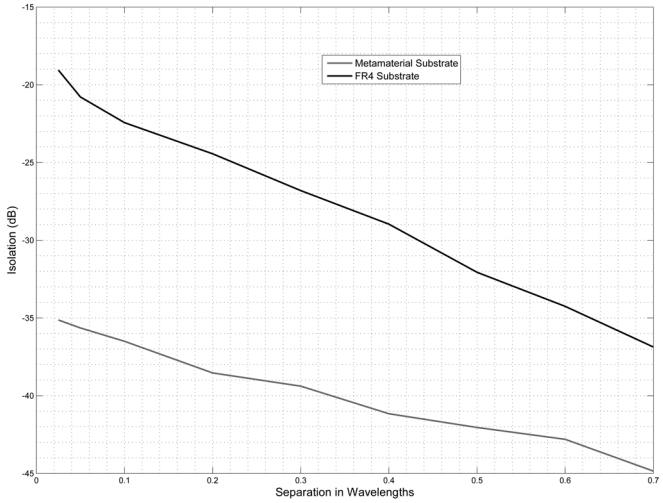

Fig. 10. Measured mutual coupling between the antenna elements for different antenna spacing for the metamaterial and FR4 substrate antenna arrays.

MEG of an antenna is evaluated by considering the mean received signal power by the test antenna and a reference antenna while they traverse a random route which is representative of the environment for which the MEG is considered to be valid. MEG is significantly affected by the antenna's gain pattern and the radio propagation environment. In this section we analytically evaluate the MEG of the metamaterial substrate array and compare it with the FR4 substrate array for different propagation scenarios.

The following analytical expression for MEG is used in our analysis [26]:

$$\mathrm{MEG} = \int_0^{2\pi}\int_0^{\pi}\left[\frac{\mathrm{XPR}}{1+\mathrm{XPR}}G_\theta(\theta,\phi)P_\theta(\theta,\phi) + \frac{1}{1+\mathrm{XPR}}G_\phi(\theta,\phi)P_\phi(\theta,\phi)\right]\sin\theta d\theta d\phi. \quad (5)$$

Fig. 9 shows the MEG of the metamaterial-substrate antenna referenced to the FR4 antenna's MEG. The same values for m_H, m_V, σ_V, and σ_H were assumed as in the previous section. As one would expect due to the significant gain differences between the antennas, the metamaterial-substrate antenna does not outperform the FR4 antenna in any XPR region. However some interesting observations can be made from this figure. The MEG of the $\lambda/20$ spaced metamaterial-substrate antenna w.r.t. the $\lambda/20$ spaced FR4 antenna is close to -2 dB. This difference is less than the measured peak gain differences seen in Fig. 6. In other words, the difference in gain becomes narrower when the antennas are operated in a mobile scenario similar to the one considered for the MEG calculations. Second, the MEG for the $\lambda/2$ spaced metamaterial-substrate antenna w.r.t. its FR4 counterpart decreases to -3 dB. However this difference in MEG is still less than the measured peak gain differences. The preceding two observations can be explained by the correlation coefficients of the antennas shown in Table IV where the closely spaced FR4 antennas suffer from high correlation compared to the metamaterial-substrate antenna.

Another observation is that there is an improvement in MEG as the cross over to positive XPR region occurs for both spacings. This MEG improvement can be explained by the higher XPD values for the metamaterial-substrate antenna shown in Table III. In the positive XPR region, most of the incident power is vertically polarized and proportionally, the metamaterial-substrate antenna can better capture this power than the FR4 antenna resulting in an increase in MEG.

VI. Channel Measurements and Results

The performance of the designed metamaterial-substrate antenna array as well as the FR4 array was evaluated in terms of achievable channel capacity by taking measurements on a 2×2 MIMO testbed. The measurements were performed in two different indoor environments. One was a medium sized laboratory (test environment I). The laboratory is 20 m long, 8 m wide, and 4 m high. The lab has several cubicles segmented by metallic walls and has other typical laboratory furniture, electronic equipment, and cabling scattered throughout the room. A single transmitter location was chosen. Channel measurements were performed for six receiver locations. The second environment was a medium sized atrium situated inside the Bossone research building on Drexel University campus (test environment II). This space is enclosed by a combination of walls and metallic doors with the space within the atrium being practically empty. Channel measurements were performed for five receiver locations. The CAD layout of both the environments are shown in Fig. 11. The transmitter locations are denoted by a "TX" and the receiver positions by the corresponding number in the layout diagrams. Receiver locations were chosen so that there were a combination of both LOS and NLOS links in both environments. For all the transmitter and receiver positions in both the environments, the antennas were mounted at a height of 1.5 m.

Measurements were taken with two nodes of the HYDRA testbed [27]. The HYDRA testbed is a 2×2 MIMO orthogonal frequency division multiplexing (OFDM) communication system equipped with frequency agile transceivers operating in

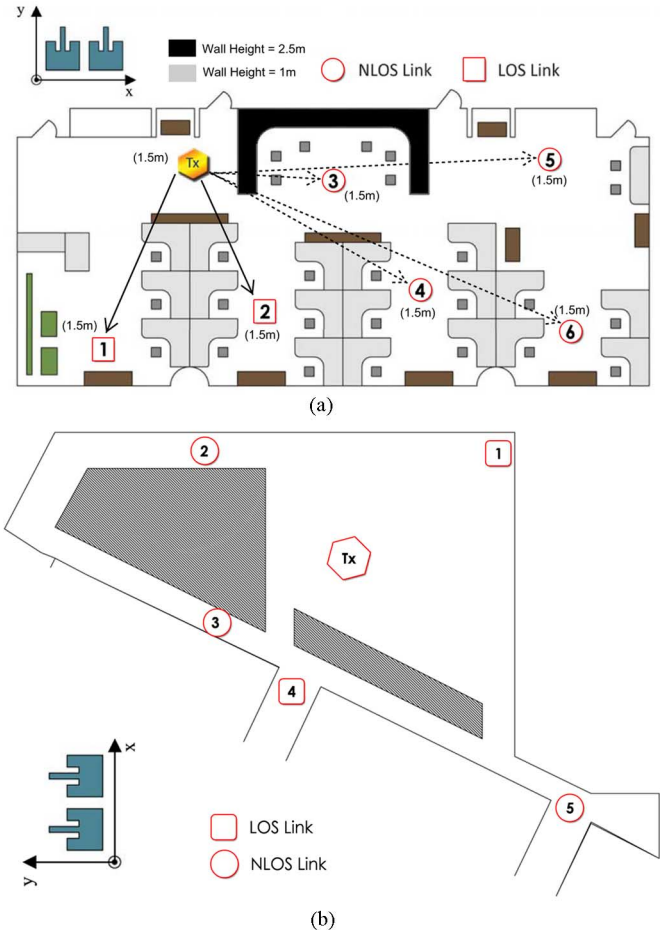

Fig. 11. 2-D CAD model of indoor (a) Test environment I. The number in the brackets indicate the height of the antennas at the particular location. The NLOS links are due to the 2.5-m partition walls which are higher than the height at which the antennas were mounted. (b) Test environment II showing the transmitter and receiver locations and the antenna array orientation.

the ISM and UNII radio bands and a baseband processing computer. The baseband chassis performs the analog to digital and digital to analog conversions required by the two transceivers. The system employs 64 sub-carriers in a 20 MHz bandwidth centered around 2.484 GHz out of which 52 sub-carriers are used for data transmission. The rest of the sub carriers are used for training.

The communication channel is assumed to be a flat fading MIMO communication channel, described by the following equation:

$$\mathbf{y} = \mathbf{H}\mathbf{x} + \mathbf{n} \tag{6}$$

where $\mathbf{x}$ is the $N_T \times 1$ transmitted signal vector, $\mathbf{y}$ is the $N_R \times 1$ received signal vector, $\mathbf{H}$ is the $N_R \times N_T$ channel transfer matrix, N_R and N_T are the number of receivers and transmitters, respectively, and $\mathbf{n}$ denotes additive white Gaussian noise.

Measurements were performed for six different array configurations: metamaterial-substrate antenna array with inter-element spacing of $\lambda/20, \lambda/10$ and $\lambda/2$ and the same spacing repeated with the FR4 antenna array for test environment I and four different array configurations: metamaterial-substrate antenna array with inter-element spacing of $\lambda/10$ and $\lambda/2$ and the same spacing repeated with the FR4 antenna array for test environment II. The $\mathbf{H}$ matrices obtained for each link were normalized with respect to the corresponding $\lambda/2$ spaced FR4 antenna array configuration in order to remove the difference in path losses among the different array configurations. This Frobenius normalization factor is defined as [4]

$$N_F = \sqrt{\frac{\left\|\mathbf{H}_{(\mathbf{0.5}\lambda),(\mathbf{FR4})}\right\|^2}{N_R N_T}}. \tag{7}$$

The channel capacity for each array configuration was computed using the normalized matrices as follows [28]:

$$C = \frac{1}{N_{\mathrm{ch}}} \sum_{i=1}^{N_{\mathrm{ch}}} \log_2 \left[\det \left(\mathbf{I}_{N_R} + \frac{\mathrm{SNR}}{N_T} \mathbf{H_i} \mathbf{H_i}^{\dagger} \right) \right] \tag{8}$$

where $\mathbf{I}_{N_R}$ is the $N_R \times N_R$ identity matrix, SNR is the signal-to-noise ratio. $N_{\mathrm{ch}} = 200$ is the number of channel realizations measured at each receiver position, $\mathbf{H_i}$ is the normalized channel matrix corresponding to the ith channel realization, and $\dagger$ denotes the complex conjugate transpose operation.

The average capacities achieved as a function of signal to noise ratio over multiple channel realizations and different links for the six different array configurations at the edge frequency of 2.474 GHz for test environment I are shown in Fig. 12. Due to their much higher gain, the FR4 substrate antennas outperform the metamaterial-substrate antenna. However, it is important to note that the performance of the metamaterial-substrate antenna is relatively unchanged with different inter-element spacing. The $\lambda/2$ spaced metamaterial-substrate antenna array shows only a 0.4 bit/Hz/s maximum improvement over its $\lambda/20$ spaced array whereas the $\lambda/2$ spaced FR4 array shows a 2 bit/Hz/s improvement. This unchanging capacity can be explained by looking at Fig. 10 and Table IV where mutual coupling and the correlation coefficients vary comparatively little with increasing inter-element spacing for the metamaterial array. For a given throughput requirement, this significant result makes the metamaterial-substrate antenna a highly suitable candidate for a MIMO system because it can be spaced very closely together without sacrificing performance. This close spacing reinforces the already small structure of the metamaterial-substrate antenna, leading to a significant reduction in antenna footprint in the system.

Similar capacity results for test environment II at the same frequency is shown in Fig. 13. Again, the same trends are present. The difference in capacity performance remains within a very close margin between the $\lambda/10$ and $\lambda/2$ spaced metamaterial-substrate antenna arrays.

Fig. 14 shows the capacities achieved by the metamaterial-substrate antenna array at the different sub-carrier frequencies of the OFDM system at 10-dB SNR. The frequency span of the OFDM system is 20 MHz centered around 2.484 GHz. As it can be seen, the capacity is a function of frequency. This can be attributed to the small scale propagation effects at different frequencies combined with the subtle gain differences within this

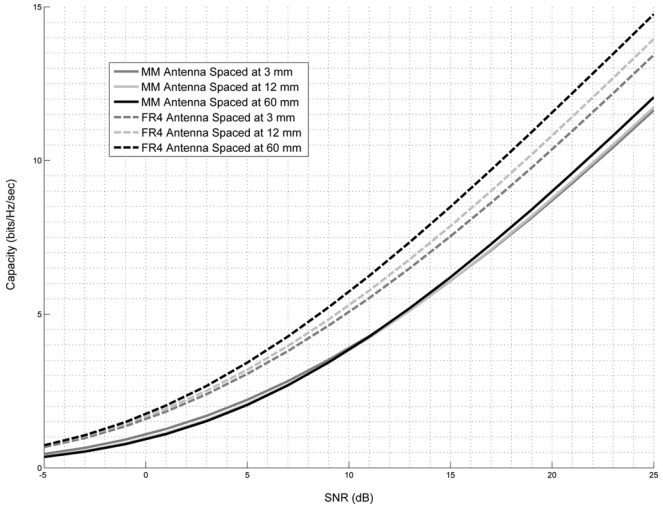

Fig. 12. Test environment I: Average channel capacity as a function of SNR for the metamaterial and FR4 substrate antenna arrays for different inter-element spacing.

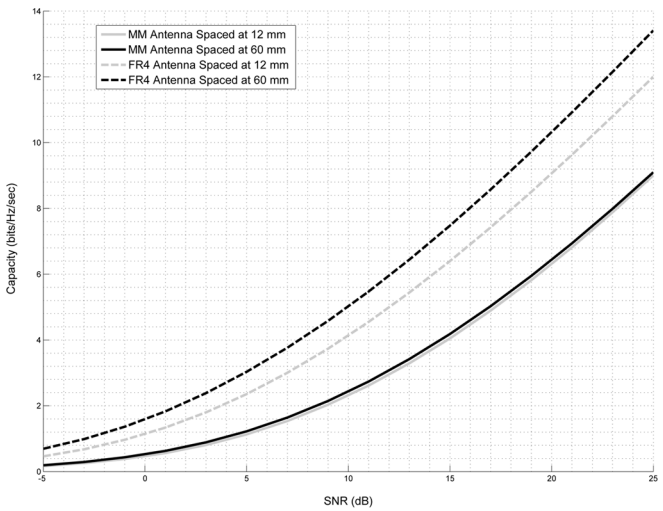

Fig. 13. Test environment II: Average channel capacity as a function of SNR for the metamaterial and FR4 substrate antenna arrays for different inter-element spacing.

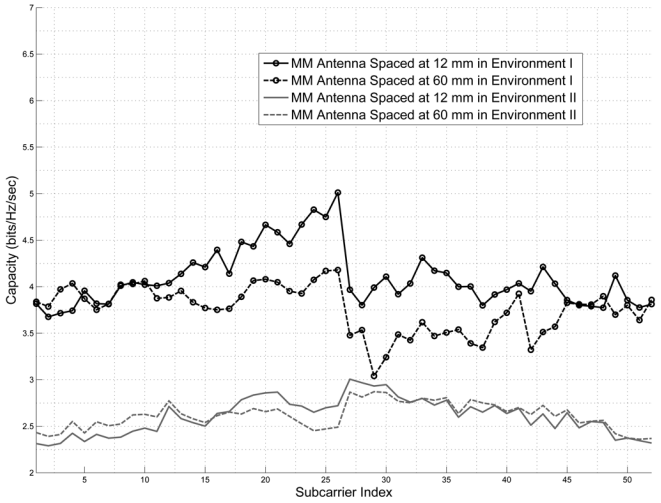

Fig. 14. Average OFDM sub-carrier capacity for the metamaterial and FR4 substrate antenna arrays with different inter-element spacing. $\mathrm{SNR} = 10$ dB.

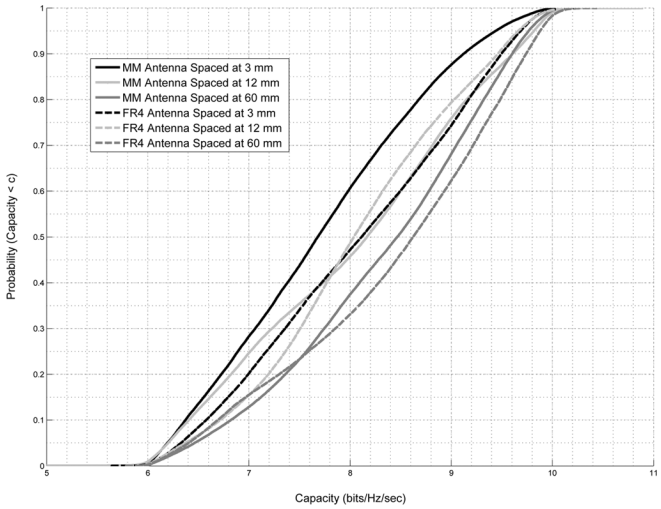

Fig. 15. CDF of channel capacity for the metamaterial and FR4 substrate antenna arrays for different inter-element spacing after normalizing for efficiency and gain mismatch effects.

band as listed in Table II. Yet the figure shows that the achievable capacity does approximately vary about a mean line within the 20-MHz frequency range.

Finally, to compare the two antenna substrates with normalizations to remove relative gain and efficiency effects, a cumulative distribution function (cdf) was assembled using the capacities computed for all links and all sub-carriers in test environment 1. The channel matrices for each antenna array configuration had its own normalization factor. The Frobenius normalization factor in this case is defined as

$$N_{F,\mathrm{Configuration,Frequency}} = \sqrt{\frac{\|H_{\mathrm{Configuration,Frequency}}\|^2}{N_R N_T}}. \tag{9}$$

The cdf results are shown in Fig. 15 for a SNR of 10 dB. For a given inter-element spacing, it can be seen that the two arrays show similar performance. For any given outage probability, the metamaterial-substrate antenna array either outperforms the FR4 array or lies within a 1 bit/Hz/s difference. These results confirm the fact that the performance gap between metamaterial and FR4 substrates in Fig. 12 can be attributed to gain and efficiency factors.

VII. Conclusion

We have compared the correlation characteristics, mean effective gain and capacity of a 2×2 MIMO communication system that employed a metamaterial-substrate antenna array to that of a system that employed patch antennas built on a conventional FR4 substrate. The metamaterial-substrate antenna array showed significantly less correlation between its elements in a typical indoor environment scenario for different inter-element spacings. This result also manifested itself in the measured channel capacities in two different indoor environments where the capacity improvement did not change significantly with

increasing inter-element spacing. Although the gain values were significantly higher for the reference FR4 antenna, the difference in analytical mean effective gain was significantly reduced due to the better polarization discrimination properties of the metamaterial substrate. When normalized for gain and efficiency effects, the metamaterial-substrate antenna array showed very similar capacity gains to those of the FR4 array. Analysis also showed that the efficiency of the metamaterial-substrate antenna can be improved with better choices for the host dielectric material. This makes the metamaterial substrate a very cost-effective solution to miniaturize antennas in future communication systems.

Our results show that the designed metamaterial-substrate antenna array is a good candidate for space constrained MIMO systems. With further improvements to its efficiency and gain, a topic of ongoing investigation, a metamaterial-substrate antenna array could become an ideal candidate for future MIMO systems.

ACKNOWLEDGMENT

The authors would like to thank D. Piazza for his helpful comments and suggestions. They would also like to acknowledge J. Kountouriotis for his help with data analysis.

REFERENCES

[1] G. J. Foschini and M. J. Gans, "On limits of wireless communications in a fading environment when using multiple antennas," *Wireless Personal Commun.*, vol. 6, no. 3, pp. 311–335, 1998.

[2] A. Forenza and R. Heath, Jr., "Benefit of pattern diversity via two-element array of circular patch antennas in indoor clustered MIMO channels," *IEEE Trans. Commun.*, vol. 54, no. 5, pp. 943–954, May 2006.

[3] A. Tulino, A. Lozano, and S. Verdu, "Impact of antenna correlation on the capacity of multiantenna channels," *IEEE Trans. Information Theory*, vol. 51, no. 7, pp. 2491–2509, Jul. 2005.

[4] M. Jensen and J. Wallace, "A review of antennas and propagation for MIMO wireless communications," *IEEE Trans. Antennas Propag.*, vol. 52, no. 11, pp. 2810–2824, Nov. 2004.

[5] J. Gianvittorio and Y. Rahmat-Samii, "Fractal antennas: A novel antenna miniaturization technique, and applications," *IEEE Antennas Propag. Mag.*, vol. 44, no. 1, pp. 20–36, Feb. 2002.

[6] R. G. P. Bhartia, I. Bahl, and A. Ittipiboon, *Microstrip Antenna Design Handbooks.*. Norwell, MA: Artech House, 2000.

[7] S. Bokhari, J.-F. Zurcher, J. Mosig, and F. Gardiol, "A small microstrip patch antenna with a convenient tuning option," *IEEE Trans. Antennas Propag.*, vol. 44, no. 11, pp. 1521–1528, Nov. 1996.

[8] R. Chair, K.-M. Luk, and K.-F. Lee, "Measurement and analysis of miniature multilayer patch antenna," *IEEE Trans. Antennas Propag.*, vol. 50, no. 2, pp. 244–250, Feb. 2002.

[9] Z. Du, K. Gong, J. Fu, B. Gao, and Z. Feng, "A compact planar inverted-f antenna with a pbg-type ground plane for mobile communications," *IEEE Trans. Veh. Technol.*, vol. 52, no. 3, pp. 483–489, May 2003.

[10] V. Voipio, J. Ollikainen, and P. Vainikainen, "Quarter-wave patch antenna with 35% bandwidth," in *Proc. IEEE Antennas Propag. Soc. Int. Symp.*, Jun. 1998, vol. 2, pp. 790–793, vol.2.

[11] H. K.-M. Sigalas, M. M. , and R. Biswas, "Theoretical study of dipole antennas on photonic band-gap materials," *Microw. Opt. Technol. Lett.*, vol. 13, no. 4, pp. 205–209, 1996.

[12] E. Altshuler and D. Linden, "Wire-antenna designs using genetic algorithms," *IEEE Antennas Propag. Mag.*, vol. 39, no. 2, pp. 33–43, Apr. 1997.

[13] A. Lai, T. Itoh, and C. Caloz, "Composite right/left-handed transmission line metamaterials," *IEEE Microw. Mag.*, vol. 5, no. 3, pp. 34–50, Sep. 2004.

[14] N. Engheta and R. Ziolkowski, *Metamaterial, Physics and Engineering Explorations.*. New York: Wiley Interscience, 2006.

[15] A. Sanada, M. Kimura, I. Awai, C. Caloz, and T. Itoh, "A planar zeroth-order resonator antenna using a left-handed transmission line," in *Proc. 34th Eur. Microw. Conf.*, Oct. 2004, vol. 3, pp. 1341–1344.

[16] S. Enoch, G. Tayeb, P. Sabouroux, N. Guérin, and P. Vincent, "A metamaterial for directive emission," *Phys. Rev. Lett.*, vol. 89, no. 21, p. 213902, Nov. 2002.

[17] S. Lim, C. Caloz, and T. Itoh, "Metamaterial-based electronically controlled transmission-line structure as a novel leaky-wave antenna with tunable radiation angle and beamwidth," *IEEE Trans. Microw. Theory Tech.*, vol. 53, no. 1, pp. 161–173, Jan. 2005.

[18] R. Ziolkowski and A. Erentok, "Metamaterial-based efficient electrically small antennas," *IEEE Trans. Antennas Propag.*, vol. 54, no. 7, pp. 2113–2130, Jul. 2006.

[19] K. Buell, H. Mosallaei, and K. Sarabandi, "A substrate for small patch antennas providing tunable miniaturization factors," *IEEE Trans. Microw. Theory Tech.*, vol. 54, no. 1, pp. 135–146, Jan. 2006.

[20] "HFSS v11.0," Ansoft Co., Pittsburgh, PA [Online]. Available: http://www.ansoft.com/products/hf/hfss/

[21] D. R. Smith, D. C. Vier, T. Koschny, and C. M. Soukoulis, "Electromagnetic parameter retrieval from inhomogeneous metamaterials," *Phys. Rev. E*, vol. 71, no. 3, p. 036617, Mar. 2005.

[22] C. A. Balanis, *Antenna Theory: Analysis and Design.*. New York: Wiley, 1997.

[23] L. M. Correia, *Wireless Flexible Personalized Communications.*. New York: Wiley, 2001.

[24] T. Taga, "Analysis of correlation characteristics of antenna diversity in land mobile radio environments," *Electron. Commun. Japan (Part I: Commun.)*, vol. 74, no. 8, pp. 101–116, 1991.

[25] K. Kalliola, K. Sulonen, H. Laitinen, O. Kivekas, J. Krogerus, and P. Vainikainen, "Angular power distribution and mean effective gain of mobile antenna in different propagation environments," *IEEE Trans. Veh. Technol.*, vol. 51, no. 5, pp. 823–838, Sep. 2002.

[26] T. Taga, "Analysis for mean effective gain of mobile antennas in land mobile radio environments," *IEEE Trans. Veh. Technol.*, vol. 39, no. 2, pp. 117–131, May 1990.

[27] K. Mandke, S. Choi, G. Kim, R. Grant, R. Daniels, W. Kim, R. Heath, and S. Nettles, "Early results on hydra: A flexible MAC/PHY multihop testbed," in *Proc. VTC2007-Spring. IEEE 65th Veh. Technol. Conf.*, Apr. 2007, pp. 1896–1900.

[28] H. Bolcskei, D. Gesbert, and A. Paulraj, "On the capacity of OFDM-based spatial multiplexing systems," *IEEE Trans. Commun.*, vol. 50, no. 2, pp. 225–234, Feb. 2002.

Prathaban Mookiah (S'05) received the B.Sc. degree (first class honors) in electrical and electronic engineering from the University of Peradeniya, Sri Lanka, in 2003. He is currently working toward the Ph.D. degree in the Wireless Systems Laboratory, Drexel University, Philadelphia, PA.

From 2004 to 2005, he worked as a Research Engineer at the Dialog—University of Moratuwa Mobile Communications Research Laboratory, Sri Lanka. His research interests include MIMO communication systems, reconfigurable antennas, metamaterials RF applications, and RFID systems.

Kapil R. Dandekar (S'95–M'01–SM'07) received the B.S. degree in electrical engineering from the University of Virginia, Charlottesville, in 1997 with specializations in communications and signal processing, applied electrophysics, and computer engineering and the M.S. and Ph.D. degrees in electrical and computer engineering from the University of Texas at Austin in 1998 and 2001, respectively.

From 1993–1997, he worked at the U.S. Naval Research Laboratory. In 2001, he joined the Electrical and Computer Engineering Department at Drexel University, Philadelphia, PA. He is currently an Associate Professor and the Director of the Drexel Wireless Systems Laboratory (DWSL). DWSL has been supported by the U.S. National Science Foundation, Army CERDEC, National Security Agency, Office of Naval Research, and private industry. His current research interests involve MIMO ad hoc networks, reconfigurable antennas, software defined radio, free space optical communications, ultrasonic communications, and sensor networks.

Prof. Dandekar has published articles in several journals including the IEEE TRANSACTIONS ON ANTENNAS AND PROPAGATION, the IEEE TRANSACTIONS ON WIRELESS COMMUNICATIONS, the IEEE TRANSACTIONS ON COMMUNICATIONS, the IEEE TRANSACTIONS ON VEHICULAR TECHNOLOGY, and the IEEE ELECTRONICS LETTERS. He currently serves on the editorial board of *IEEE Expert Now*, and also serves on the IEEE Educational Activities Board.